Microstructure and Mechanical Properties of Pulsed Laser Beam Welded Ti-2Al-1.5Mn Titanium Alloy Joints

Xiuyang Fang, Hong Liu, and Jianxun Zhang

The microstructure and mechanical properties in the pulsed laser beam welded joints of Ti-2Al-1.5Mn titanium alloy thin sheet were investigated in this study. The results show that the original α + β-phases and the transformed α + α′-phases are found in the partially transformed heat-affected zone (HAZ) together with the remaining β-phase, and the microhardness gradually enhances in the region as the result of the increase of α′-phase. The martensitic α′-phase and the remaining β-phase are detected in the fully transformed HAZ and the fusion zone (FZ), and the highest microhardness is found in these regions in virtue of the dominant α′-phase structure. The fine α′-phase appeared in the FZ results in higher average microhardness at high welding speed. Moreover, similar to the results of microhardness test, the tensile test results mean that the HAZ and FZ are stronger than the base metal (BM). Therefore, pulsed laser beam welding is feasible for joining thin sheet of Ti-2Al-1.5Mn titanium alloy.

1. Introduction

The dual phase titanium alloys have been widely applied in the aerospace, chemical, and medical industries because of the high specific strength, excellent high-temperature mechanical properties, good corrosion resistance, and excellent biocompatibility (Ref 1, 2), e.g., for the aviation jet mouth skin structure. Thus, their welding and joining technologies have attracted considerable interests in order to apply these materials for complex component (Ref 3), and many welding methods such as gas tungsten arc welding (Ref 4-6), laser beam welding (Ref 5-11), electron beam welding (Ref 12, 13), friction welding (Ref 14), and laser hybrid welding (Ref 15) have already been developed. Most have focused on the laser beam welding technique due to the small welding deformation, narrow weld zone, fine microstructure in welded joint as well as high-volume production with precision, speed, and reliability in application (Ref 6, 10). A continuous-wave mode laser has advantages for welding thick plate when employing kilowatt level laser power. However, a pulsed-wave mode laser, effectively restricting the weld heat input by intermittent pulsed laser power, allows melting and solidification to take place consecutively (Ref 16, 17). Pulsed Nd:YAG laser welding usually provides benefits such as lower heat input, less deformation, and narrower weld bead and heat-affected zone (Ref 18, 19). The solidification time in pulsed Nd:YAG laser is even shorter than that in a continuous laser beam welding or electron beam welding. Therefore, a pulsed-wave mode laser is more suitable for welding thin sheet (Ref 6, 20).

In the present study, the pulsed laser beam welding of Ti-2Al-1.5Mn titanium alloy thin sheet was carried out, the microstructures in the welded joints were investigated, and the relationship between the microstructures and mechanical properties was discussed in detail.
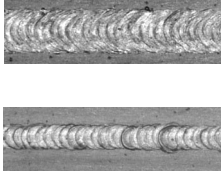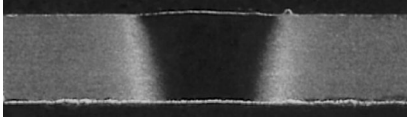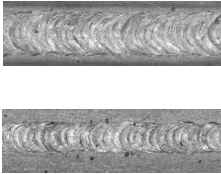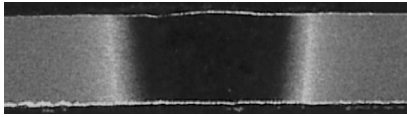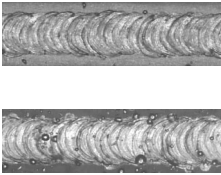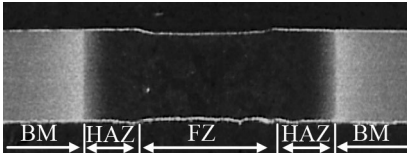
2. Experimental

The as-received material was the Ti-2Al-1.5Mn titanium alloy thin sheet with 0.8 mm thickness. The workpieces were bead-on-plate welded by a JHM-1GXY-400X pulsed Nd:YAG laser beam welding system. During welding, the pulse duration and repetition rate were fixed at 5.5 ms and 20 Hz, the pulse energies ranged from 5.6 to 9.5 J, and the welding speeds changed from 270 to 530 mm/min. Accordingly, the peak powers from 1.02 to 1.73 kW and the average power from 112 to 190 W were selected in this investigation. The average laser beam power was measur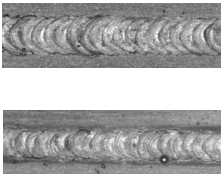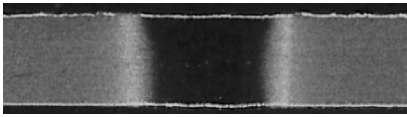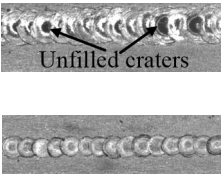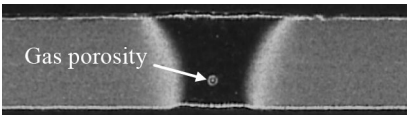ed by a handheld laser power meter under various welding conditions. Both the top and bottom surfaces of the welded joints were shielded by high-purity argon gas with a flow rate of 20 L/min to minimize the surface oxidation.

After welding, the cross sections were mechanically polished using water abrasive papers, and then were electropolished at room temperature for 15 s under a potential of 25 V in a solution containing perchloric acid, n-butyl alcohol, and methanol at a volume ratio of 1:7:12. The macrostructures of the polished cross sections were obtained by an image measuring instrument (VMS-1510G; Rational Co., Ltd.). Finally, the polished cross sections were etched in a solution comprising hydrofluoric acid, nitric acid, and distilled water at a volume ratio of 1:1:48. The microstructures of the etched cross sections were observed by an optical microscope (OM; Nikon ECLIPSE MA200; Nikon Corp.) and a scanning electron microscope (SEM; VEGAII-XMU; TESCAN Corp.). Composition analyses of different

Xiuyang Fang, Hong Liu, and Jianxun Zhang, State Key Laboratory for Mechanical Behavior of Materials, Xi'an Jiaotong University, Xi'an 710049, China. Contact e-mail: fangxiuyang@stu.xjtu.edu.cn.

Table 1 Bead appearances and macrostructures in the welded joints under various welding conditions

Pulse energy, J	Peak power, kW	Average power, W	Welding speed, mm/min	Face/back bead appearance	Macrostructure
5.6	1.02	112	270		
7.3	1.33	146	270		
9.5	1.73	190	270		BM HAZ FZ HAZ BM
7.3	1.33	146	400		
7.3	1.33	146	530	Unfilled craters	Gas porosity

positions were performed by an energy-dispersive x-ray spectroscopy system (EDS; Oxford Instruments). More detailed microstructural information was obtained by a transmission electron microscope (TEM; JEM-200CX; JEOL Ltd.). The TEM specimens of different zones were initially cut using a linear precision saw (ISOMET 4000; Buehler Ltd.) parallel to the welding direction from the cross section, then mechanically polished using water abrasive papers up to 0.08 mm, and finally wrapped in a copper disk with a hole in the center for the ion milling (GATAN-691; Gatan Inc.). The hardness tests were measured by a hardness testing machine (HXD-1000TMC; Shanghai Taiming Optical Instrument Co., Ltd.) under a load of 300 g for a dwell time of 15 s with an interval of 0.1 mm. The tensile properties were evaluated by means of a tensile testing machine (Instron 1195; Instron Corp.) at room temperature with

a constant extension speed of 2 mm/min. Fracture morphology of tensile specimen was observed with SEM.

3. Results and Discussion

3.1 Bead Appearances and Macrostructures in the Welded Joints

The bead appearances and macrostructures in the welded joints under various welding conditions are given in Table 1. The ripple welds with silvery white surfaces are observed after welding, as shown in Table 1. During pulsed laser beam welding, the new keyhole is formed with the laser spot moving, and the liquid metal in front of welding pool flows back and

fills the old keyhole at the same time. When welded at high welding speed, the distance between two adjacent laser spots increases, and thus the liquid metal cannot fill the old keyhole sufficiently. For this reason, the unfilled craters can be found in the joint at 530 mm/min welding speed. On the other hand, the keyhole is unstable in the welding condition, and it easily induces the formation of gas porosity. Increasing the repetition rate can decrease the distance between two adjacent laser spots, which probably avoids the unfilled craters at the same welding speed. The macrostructures before etching and after electropolishing display the narrow and symmetric shapes. A keyhole type of penetration is detected in the welds, and the fully penetrated welds are obtained in this investigation. The width of welded joints notably increases with the pulse energy increasing, whereas it decreases with the increase of welding speed. Moreover, the welded joint consists of the BM, HAZ, and FZ.

3.2 Microstructures in the Welded Joints

The microstructure of the typical welded joint during pulsed laser beam welding is shown in Fig. 1. It can be seen that the microstructures in the HAZ near the BM are dissimilar to those in the HAZ near the FZ. The prior β-grains in the FZ show the columnar morphology and grow epitaxially from the prior β-grains in the HAZ near the FZ. Figure 2 shows the microstructures of the different regions in the welded joint under the welding condition of 5.6 J and 270 mm/min. As seen from Fig. 2a, both the equiaxed phase with the composition of 97.9Ti-1.4Al-0.7Mn (wt.%) and the granular phase with the composition of 91.4Ti-0.6Al-8.0Mn are detected in the BM. The concentration of Al suggests that the equiaxed phase is the α-phase, and the concentration of Mn implies that the granular phase is the β-phase. The α- and β-phases have the hexagonal close-packed (HCP) crystal structure and the body-centered cubic (BCC) crystal structure, respectively. As shown in Fig. 2b, the original α-phase (97.6Ti-1.3Al-1.1Mn), original β-phase (93.6Ti-0.9Al-5.5Mn), transformed α-phase, and the martensitic α′-phase are observed in the HAZ near the BM.
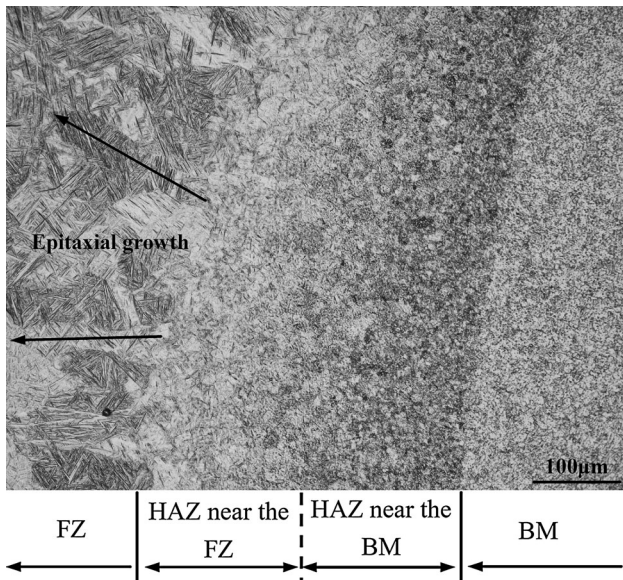

Fig. 1 Microstructure of the typical welded joint during pulsed laser beam welding
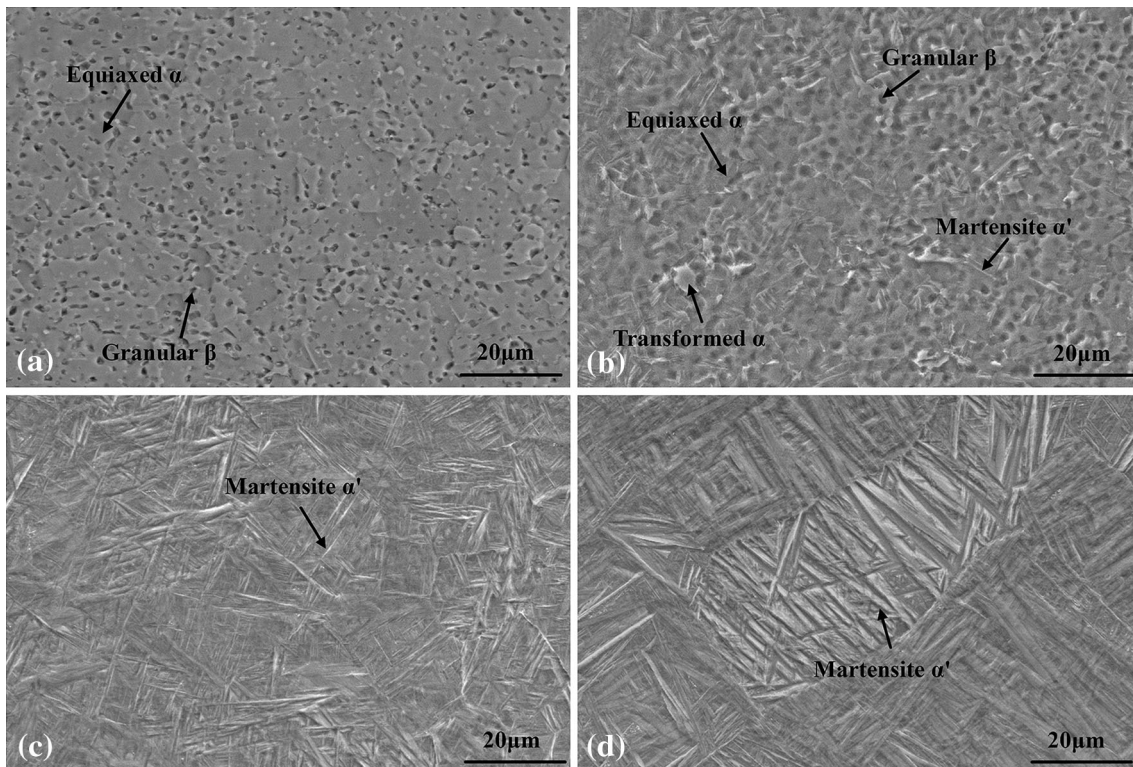

Fig. 2 Microstructures of the different regions in the welded joint under the welding condition of 5.6 J and 270 mm/min: (a) BM; (b) partially transformed HAZ; (c) fully transformed HAZ; and (d) FZ
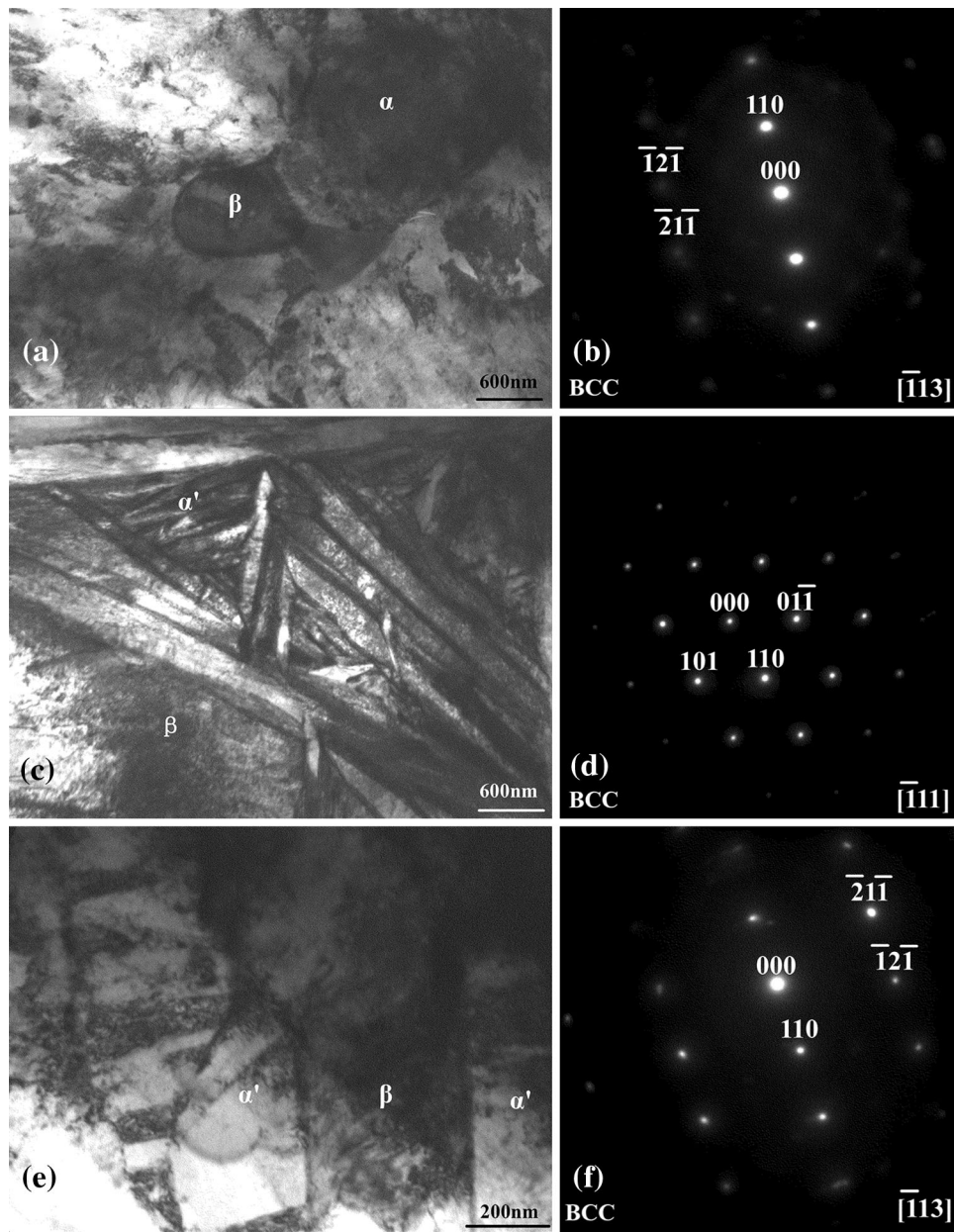
Fig. 3 TEM images of the different regions in the welded joint under the welding condition of 9.5 J and 270 mm/min: (a) BM; (b) the corresponding SAED pattern of β-phase in the BM; (c) HAZ; (d) the corresponding SAED pattern of β-phase in the HAZ; (e) FZ; and (f) the corresponding SAED pattern of β-phase in the FZ

For this reason, the HAZ near the BM can be considered to be the partially transformed HAZ. As shown in Fig. 2c, the dominant α′-phase is found in the HAZ near the FZ. The absence of the original α- and β-phases indicates that the HAZ near the FZ is the fully transformed HAZ. Figure 2d presents the microstructure of the FZ; it shows that the regnant α′-phase is also depicted in the FZ. Compared with the partially transformed HAZ, the transformed α-phase is not observed in the fully transformed HAZ and FZ. The phenomenon is ascribed to the increase of cooling rate with the position moving from the HAZ to FZ, and the martensitic transformation is predominant in the fully transformed HAZ and FZ during phase transformation after solidification. Moreover, as shown in Fig. 2c and d, the prior β-phase in the fully

transformed HAZ shows the equiaxed morphology, which distinctly differs from the columnar morphology of prior β-phase in the FZ.

It should be pointed out that most of the prior β-phase has transformed into the product α′- and/or α-phases in the HAZ and FZ, which has been discussed by Javidrad (Ref 21). However, the remained β-phase still exists in these regions after phase transformation. Figure 3 exhibits the TEM images of the different regions in the welded joint under the welding condition of 9.5 J and 270 mm/min. As shown in Fig. 3a and b, the β-phase having granular-like structure appears in the BM, and displays the BCC crystal structure with [−113] zone axis. As seen from Fig. 3c to f, the remained β-phases with lath-like structure are formed in the HAZ and FZ, which exhibit the
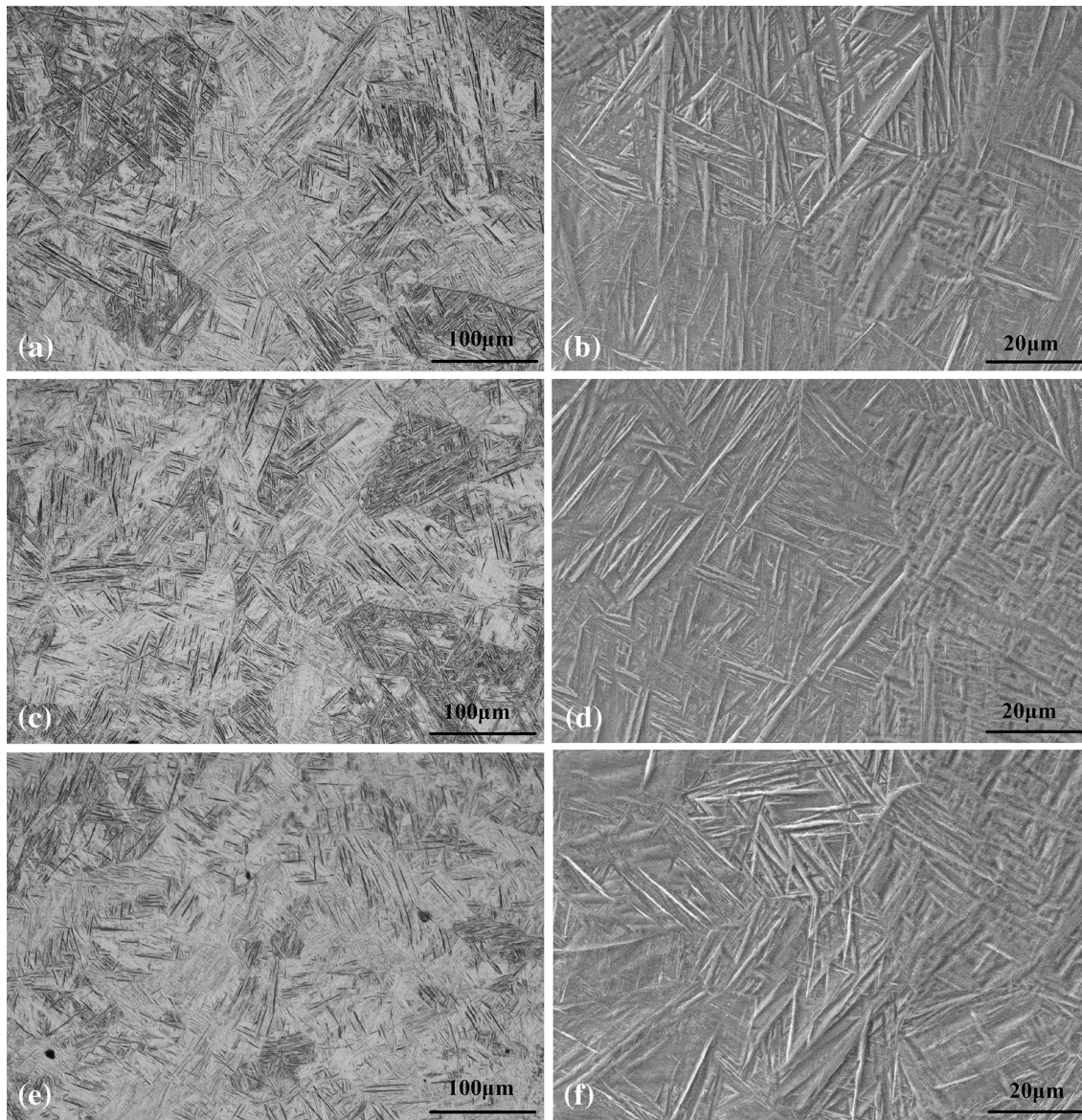
Fig. 4 Microstructures of the FZs in the welded joints under various welding speeds: (a), (b) 7.3 J and 270 mm/min; (c), (d) 7.3 J and 400 mm/min; and (e), (f) 7.3 J and 530 mm/min

BCC crystal structure with $[-111]$ and $[-113]$ zone axes, respectively. In addition, the needle-like martensitic α'-phase with the approximate width of 300 nm is presented in the HAZ and FZ. The existence of remaining β-phase probably suggests the fact that the finishing temperature of martensitic transformation for Ti-2Al-1.5Mn titanium alloy is below room temperature, similar to the Ti6Al4 V titanium alloy (Ref 22).

In order to investigate the effect of welding speed on the microstructures in the FZs, more detailed microstructures in the welded joints under various welding speeds were acquired using OM and SEM. As shown in Fig. 4, the prior β-grains of the FZs at high temperature mainly exhibit the columnar grain morphology after solidification, and gradually become fine with increasing welding speed; similar result was observed by Costa et al. (Ref 23). The martensitic α'-phases of the FZs develop from the prior β-grains during phase transformation after solidification. The martensitic α'-phase is found to be coarse at low welding speed (270 mm/min) and it becomes fine at high

welding speed (530 mm/min). The effect of pulse energy on the microstructures consists with that of welding speed. The result is associated with the fact that the cooling rate in the FZ increases with the increase of welding speed and/or the decrease of pulse energy (Ref 24, 25).

3.3 Mechanical Properties of the Welded Joints

The microhardness distributions of the welded joints under various welding conditions are shown in Fig. 5. The location of the microhardness analysis is given in the top part, the average microhardness of the FZ is displayed in the middle part, and the boundary between the partially and fully transformed HAZs is described by the dotted line. The microhardness in the partially transformed HAZ gradually enhances with the position moving from the BM to HAZ, the highest microhardness is found in the fully transformed HAZ and FZ, and the average microhardness in the fully transformed HAZ is close to that in the FZ. Additionally,
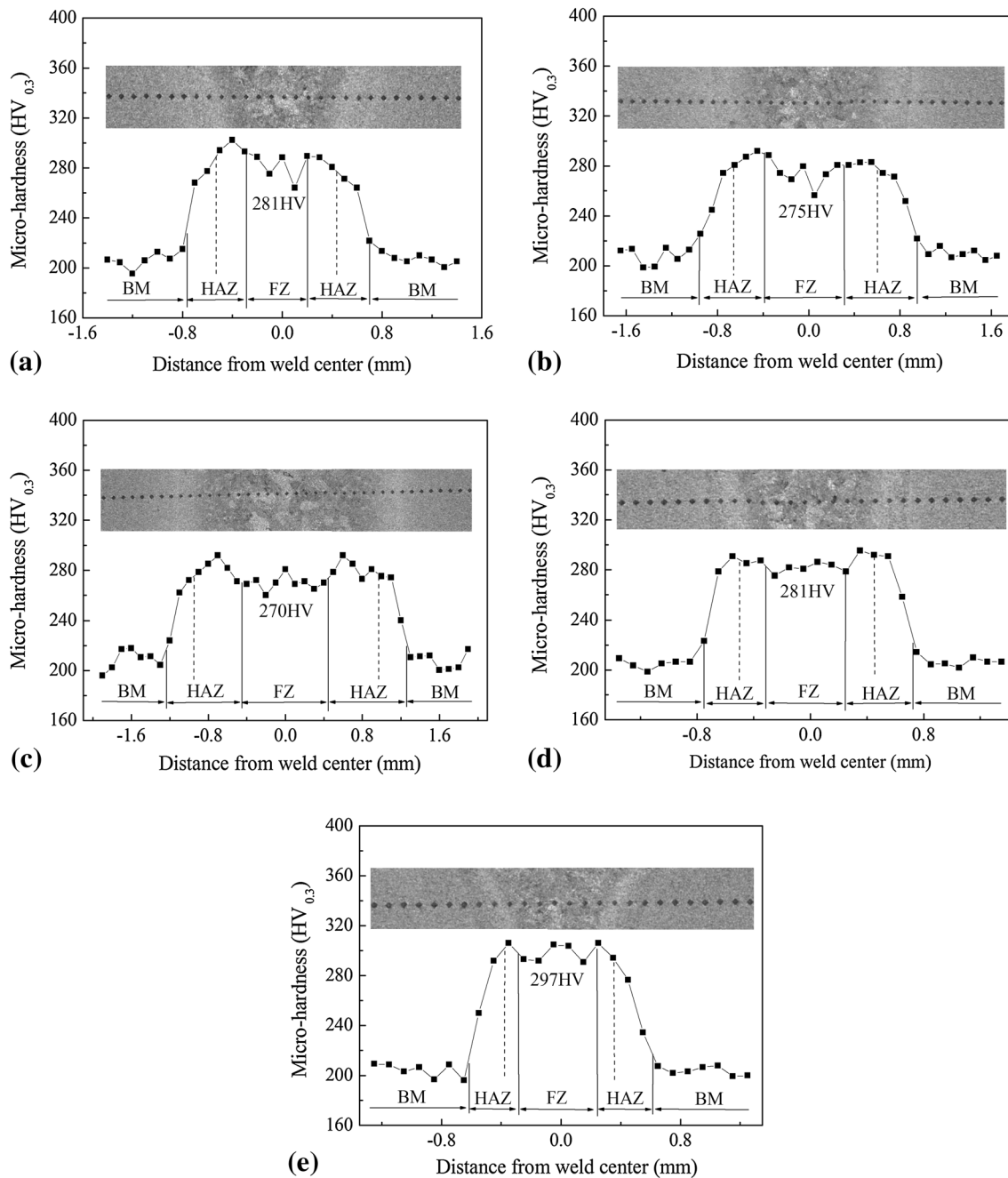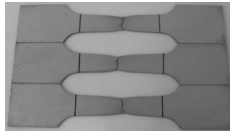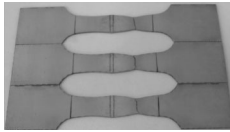
Fig. 5 Microhardness distributions of the welded joints under various welding conditions: (a) 5.6 J and 270 mm/min; (b) 7.3 J and 270 mm/min; (c) 9.5 J and 270 mm/min; (d) 7.3 J and 400 mm/min; and (e) 7.3 J and 530 mm/min

the average microhardness of the FZ is about 270 $HV_{0.3}$ under the welding condition of 9.5 J and 270 mm/min; it ascends with the increase of welding speed and/or the decrease of pulse energy by degrees, and is ultimately up to 297 $HV_{0.3}$ under the welding conditions of 7.3 J and 530 mm/min. The microhardness in the welded joints strongly depends on the martensitic α′-phase structure (Ref 23). The raise of microhardness in the partially transformed HAZ is evidently due to the increase of martensitic α′-phase. The β → α′ martensitic transformation dominantly occurs in the fully transformed HAZ and FZ, which leads to the highest hardness in these regions. The fine martensitic α′-phase is found in the FZ at high welding speed, and thus the average

hardness of the FZ in the welding condition is high compared with that at low welding speed. Table 2 describes the average tensile strengths, average elongations, fracture positions, and tested specimen photographs of the BM and the welded joint. The welded joint fractures at the BM and the tensile results of the welded joint are nearly accordant with those of the BM. Results of the tensile tests mean that the HAZ and FZ are strong, which is reasonably consistent with the hardness test results. Fracture surface of the tensile specimens was examined by SEM. As shown in Fig. 6, the fractographic image reveals cup and cone fractures with dimpled structures, representing that the ductile type of fracture mode occurs.

Table 2 Average tensile strengths, average elongations, fracture positions, and tested specimen photographs of the BM and welded joint

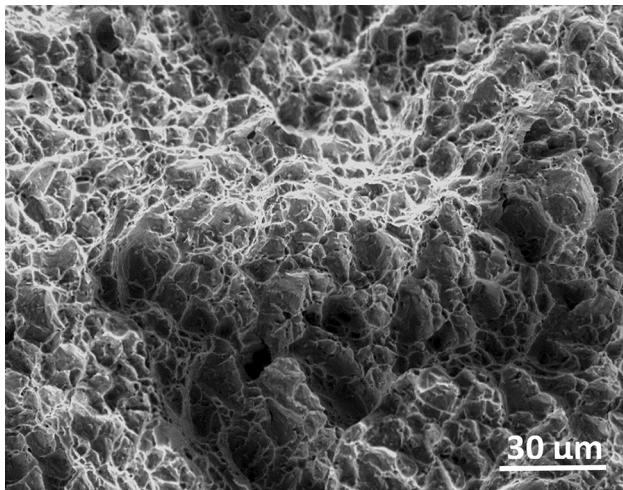| Specimen	Pulse energy, J	Welding speed, mm/min	Average tensile strength, MPa	Average elongation, %	Fracture position	Tested specimen photograph
BM	...	...	642	24	BM	
Joint	7.3	270	661	22	BM	

Fig. 6 SEM image of tensile fracture surface (broken in the BM)

4. Conclusions

The welded joints of Ti-2Al-1.5Mn titanium alloy thin sheet were prepared by pulsed laser beam welding, and the microstructure and mechanical properties of the welded joints were investigated. The main conclusions are as follows:

1. The $\beta \rightarrow a'$ martensitic transformation occurs in the partially transformed HAZ during phase transformation after solidification, and it is predominant in the fully transformed HAZ and FZ. The original a + b-phases and the transformed a + a'-phases are formed in the partially transformed HAZ together with the remaining b-phase, and the martensitic a'-phase and the remaining b-phase are detected in the fully transformed HAZ and FZ.

2. The microhardness in the partially transformed HAZ gradually enhances due to the increase of α'-phase, and the highest microhardness is found in the fully transformed HAZ and FZ. The α'-phase in the FZ becomes fine with the increase of welding speed, and the average microhardness in the region is high at high welding speed and/or low pulse energy.

3. The tensile test results indicate that the HAZ and FZ are stronger than the BM, which is consistent with the hardness test results. Fracture is ductile. According to the results, it can be stated that pulsed laser beam welding is feasible for joining thin sheet of Ti-2Al-1.5Mn titanium alloy.

References

1. C. Leyens and M. Peters, *Titanium and Titanium Alloys: Fundamentals and Applications*, Wiley-VCH, Weinheim, 2003
2. N. Poondla, T.S. Srivatsan, A. Patnaik, and M. Petraroli, A Study of the Microstructure and Hardness of Two Titanium Alloys: Commercially Pure and Ti-6Al-4 V, *J. Alloys Compd.*, 2009, **486**, p 162–167
3. W.A. Baeslack III, J.R. Davis, and C.E. Cross, Selection and Weldability of Conventional Titanium Alloys, *ASM Handbook*, *Vol 6, Welding brazing and soldering*, ASM International, Materials Park, OH, 1993, p 507–523
4. A.B. Short, Gas Tungsten Arc Welding of α + β Titanium Alloys: A Review, *Mater. Sci. Technol.*, 2009, **25**, p 09–324
5. T.S. Balasubramanian, V. Balasubramanian, and M.A. Muthumanikkam, Fatigue Performance of Gas Tungsten Arc, Electron Beam, and Laser Beam Welded Ti-6Al-4 V Alloy Joints, *J. Mater. Eng. Perform.*, 2011, **20**, p 1620–1630
6. X.L. Gao, L.J. Zhang, J. Liu, and J.X. Zhang, A Comparative Study of Pulsed Nd: YAG Laser Welding and TIG Welding of Thin Ti6Al4 V Titanium Alloy Plate, *Mater. Sci. Eng. A*, 2013, **559**, p 14–21
7. P.Q. Xu, L.J. Li, and C.B. Zhang, Microstructure Characterization of Laser Welded Ti-6AL-4 V Fusion Zones, *Mater. Charact.*, 2014, **87**, p 179–185
8. X. Li, J. Xie, and Y. Zhou, Effects of Oxygen Contamination in the Argon Shielding Gas in Laser Welding of Commercially Pure Titanium Thin Sheet, *J. Mater. Sci.*, 2005, **40**, p 3437–3443
9. E. Akman, A. Demir, T. Canel, and T. Sinmazcelik, Laser Welding of Ti6Al4 V Titanium Alloys, *J. Mater. Process. Technol.*, 2009, **209**, p 3705–3713
10. F. Caiazzo, F. Curcio, G. Daurelio, and F. Memola, Capece Minutolo, Ti6Al4 V Sheets Lap and Butt Joints Carried Out by CO_2 Laser: Mechanical and Morphological Characterization, *J. Mater. Process. Technol.*, 2004, **149**, p 546–552
11. A.S.H. Kabir, X. Cao, J. Gholipour, P. Wanjara, J. Cuddy, A. Birur, and M. Medraj, Effect of Postweld Heat Treatment on Microstructure,

Hardness, and Tensile Properties of Laser-Welded Ti-6Al-4 V, *Metall. Mater. Trans. A*, 2012, **42**, p 4171–4184

12. T. Mohandas, D. Banerjee, Y.R. Mahajan, and V.V. Kutumba Rao, Studies on Fusion Zone Fracture Behaviour of Electron Beam Welds of an α + β Titanium Alloy, *J. Mater. Sci.*, 1996, **31**, p 3769–3775

13. W. Lu, Y.W. Shi, X.Y. Li, and Y.P. Lei, Correlation Between Tensile Strength and Hardness of Electron Beam Welded TC4-DT Joints, *J. Mater. Eng. Perform.*, 2013, **22**, p 1694–1700

14. L. Zhou, H.J. Liu, P. Liu, and Q.W. Liu, The Stir Zone Microstructure and Its Formation Mechanism in Ti-6Al-4 V Friction Stir Welds, *Scripta Mater.*, 2009, **61**, p 596–599

15. C. Li, K. Muneharua, S. Takao, and H. Kouji, Fiber Laser-GMA Hybrid Welding of Commercially Pure Titanium, *Mater. Des.*, 2009, **30**, p 109–114

16. F. Malek Ghaini, M.J. Hamedi, M.J. Torkamany, and J. Sabbaghzadeh, Weld Metal Microstructure Characteristics in Pulsed Nd: YAG Laser Welding, *Scr. Mater.*, 2007, **56**, p 955–958

17. E. Assuncao and S. Williams, Comparison of Continuous Wave and Pulsed Wave Laser Welding Effects, *Opt. Laser Eng.*, 2013, **51**, p 674–680

18. Y.F. Tzeng, Process Characterisation of Pulsed Nd:YAG Laser Seam Welding, *Int. J. Adv. Manuf. Technol.*, 2000, **16**, p 10–18

19. A.V. Vicente, R.B. Jose, and R. Wagner, Pulsed Nd: YAG Laser Seam Welding of AISI, 316L Stainless Steel Thin Foils, *J. Mater. Process. Technol.*, 2010, **210**, p 1838–1843

20. M.J. Torkamany, M.J. Hamedi, F. Malek, and J. Sabbaghzadeh, The Effect of Process Parameters on Keyhole Welding with a 400 W Nd :YAG Pulsed Laser, *J. Phys. D*, 2006, **39**, p 4563–4567

21. F. Javidrad, H. Farghadani, and M. Hedari, The MPAW of Ti-3Al-2.5 V Thin Sheets and Its Effects on Mechanical and Microstructural Properties, *J. Mater. Eng. Perform.*, 2013, doi:10.1007/s11665-013-0785-7

22. M.J. Donachie, *Titanium: A Technical Guide*, ASM International Metals Park, Ohio, 1988

23. A. Costa, R. Miranda, L. Quintino, and D. Yapp, Analysis of Beam Material Interaction in Welding of Titanium with Fiber Lasers, *Mater. Manuf. Process.*, 2007, **22**, p 798–803

24. J.W. Elmer, T.A. Palmer, S.S. Babu, W. Zhang, and T. DebRoy, Phase Transformation Dynamics During Welding of Ti-6Al-4 V, *J. Appl. Phys.*, 2004, **95**, p 8327–8339

25. R.M. Miranda, G. Lopes, L. Quintino, J.P. Rodrigues, and S. Williams, Rapid Prototyping with High Power Fiber Lasers, *Mater. Des.*, 2008, **29**, p 2072–2075